Unit for Drug Research and Development, Faculty of Health Sciences, North-West University, Potchefstroom, South Africa

Preparation and evaluation of metastable solid-state forms of lopinavir

H.J.R. Lemmer, W. Liebenberg

Received October 16, 2012, accepted December 12, 2012

H.J.R. Lemmer, Internal Box 36, Private Bag X6001, Potchefstroom, 2520, South Africa
Righard.Lemmer@nwu.ac.za

Pharmazie 68: 327–332 (2013) *doi: 10.1691/ph.2013.2194*

In this work, we present the preparation and evaluation of previously unreported metastable forms of the antiretroviral drug, lopinavir. By maintaining the chemical structure, physicochemical properties like the glass transition temperature (T_g), dissolution and solubility can be readily attributed to the stability of the system. Commercially-available lopinavir was used to prepare partially amorphous crystals, semicrystalline needles, resins and glasses. The physicochemical properties of each were investigated using differential scanning calorimetry (DSC), Fourier transform infrared spectroscopy (FTIR) and powder X-ray diffraction (PXRD). Each sample's thermal and spectroscopic analyses, as well as dissolution and solubility studies were performed one month after sample preparation, for better comparability. Glass transition temperature, activation energy for global molecular mobility (ΔE_{Tg}), and activation energy for local molecular mobility (ΔE_{β}) were assessed as primary indicators for structural stability of the systems. Relating these properties to aqueous solubility revealed that each metastable form possessed its own unique equilibrium solubility. Cumulative dissolved fractions (α) were fitted against deceleratory kinetics models, and from the data hereby obtained the dissolution process was determined to followed first-order kinetics ($R^2 = 0.998$). From the rate constants, the activation energy for dissolution (ΔE_{Diss}) of each sample was calculated. The results suggest that multiple metastable solid-state forms of lopinavir can exist under similar conditions, depending on the preparation conditions.

1. Introduction

Lopinavir is a peptidomimetic antiretroviral (ARV) agent which inhibits the human immunodeficiency virus (HIV) protease enzyme from cleaving the Gag-Pol polyprotein, resulting in the production of immature, non-infectious viral particles (Safrin 2004). Its chemical structure is flexible, with 4 chiral centres, and possesses the potential to undergo extensive inter- and intramolecular hydrogen bonding. This structural flexibility enables lopinavir to adopt numerous molecular coordinates on its energy landscape, increasing the probability of preparing various amorphous and crystalline forms (Stillinger 1995). The peptidomimetic structure of lopinavir also imparts an unfavorable pharmacokinetic profile on the drug due to low aqueous solubility, poor absorption and rapid hepatobiliary elimination (Kempf et al. 1997). To address the hepatobiliary elimination, ritonavir is co-administered with lopinavir to outcompete its elimination. The poor solubility of lopinavir can be addressed by preparing amorphous forms of the drug. The high internal energy and specific volume of the amorphous state have already been reported to enhance dissolution, solubility and bioavailability (Hancock and Parks 2000; Hüttenrauch 1978). However, amorphous material is known to be inherently unstable, and will eventually crystallize into a lower energy state.

To date, the glass transition temperature (T_g) and its role with regards to formulation, storage, nucleation and crystal growth, used to be the mainstay parameter for assessing the stability of amorphous systems (Elamin et al. 1994; Levine and Slade 1988; Lordi and Shiromani 1984; Mitchell and Down 1984; Ward and Schultz 1995). However, in certain instances the T_g fails to be an accurate indicator of stability (Vyazovkin and Dranca 2007; Yoshioka et al. 2006, 2007). Recently, local molecular motions (β-relaxations) have been recognized as important determinants of the stability of amorphous systems, not only with regards to coupling with global molecular motions (α-relaxations), but also concerning crystallization at temperatures well below and close to T_g, as well as the aggregation of macromolecules (Alie et al. 2004; Alig et al. 1997; Bhugra et al. 2008; Hikima et al. 1999; Ngai 2003; Vyazovkin and Dranca 2005; Vyazovkin and Dranca 2007). An additional advantage of using β-relaxations to evaluate the stability of amorphous systems, is that it allows investigation into the effects of low temperature and low energy disturbances on the system. The energy barrier imposed by the activation energy for β-relaxation (ΔE_{β}) can therefore be seen as the first step in re-establishing the energetic equilibrium of molecular mobility in amorphous systems under stress conditions, such as heating.

Studies on amorphous material generally consist of the preparation of an amorphous sample from a fully crystalline reference, either using ball milling, spray-drying, freeze-drying or cooling of the melt, followed by a comparison between the physicochemical properties of the newly formed amorphous sample and the original crystalline material (Crowley and Zografi 2001; Dantuluri et al. 2011; Graeser et al. 2009; Grzybowska et al.

2010; Hancock et al. 1998; Mahlin et al. 2011; Vyazovkin and Dranca 2006; Weuts et al. 2003). Studies in which more than one method was used to prepare more than one metastable form are sparse (Qi et al. 2008; Surana et al. 2004). Preparation of these amorphous samples either occurs *in situ*, followed by immediate sample analysis, or the exact amount of time between the sample preparation and the analysis was not reported. It should be noted however, that maintaining storage conditions and time between preparation and analyses were not the objectives of the above mentioned studies. In this study, storage and analysis times were maintained, to explore a different avenue of amorphous stability. Commercial lopinavir was dissolved in various organic solvents under conditions similar to that of a typical recrystallization and cooled under ambient conditions to yield amorphous resins and partially amorphous crystals. Two glasses were also prepared from the melt. One was quench cooled with liquid nitrogen and the other was cooled under ambient conditions to yield glasses with different degrees of disorder (Aasland and McMillan 1994; Ediger 2000; Stillinger 1995). To evaluate the stability of each system, both α- and β-relaxations were investigated. The glasses, recrystallization products and commercial lopinavir were thermally analyzed to determine the ΔE_β, fragility (m) and strength (D) parameters. These parameters were then correlated with solubility data to investigate their relations. Dissolution data were fitted to deceleratory kinetics models, and from this data the activation energy for dissolution (ΔE_{Diss}) were obtained. To facilitate comparability, all samples were stored under similar conditions and all analyses were carried out one month after sample preparation.

2. Investigations and results

Recrystallization of lopinavir yielded crystals from acetone and ethyl acetate, semicrystalline needles from diethyl ether and resins from chloroform and dichloromethane. Two glasses were also prepared from the melt. One was quenched with liquid nitrogen (henceforth referred to as QG) and the other was allowed to cool under ambient temperature (AG). Thermal analyses indicated that commercial lopinavir is amorphous, and even the crystals obtained from acetone and ethyl acetate contained some amorphous material, as is evident from the presence of glass transitions (Fig. 1). The resin obtained from chloroform also exhibited a melting endotherm, suggesting the presence of crystallites in the amorphous matrix. The DSC results were corroborated by PXRD data (Fig. 2). Both the glasses as well as the resin obtained from dichloromethane displayed only diffuse halo bands on their PXRD diffractograms (not shown). Unlike the results from previous studies (Qi et al. 2008; Surana et al. 2004), the samples prepared in this study displayed significant differences in T_g (Table 1), indicating varying degrees of disorder between the samples.

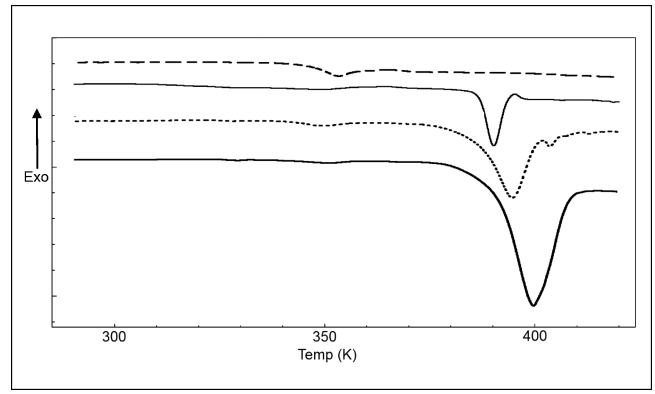

Fig. 1: DSC curves of commercial lopinavir (dashed), lopinavir resin from chloroform (thin solid), lopinavir crystals from ethyl acetate (dotted) and acetone (thick solid). Thermograms were obtained from heating at 10 K/min

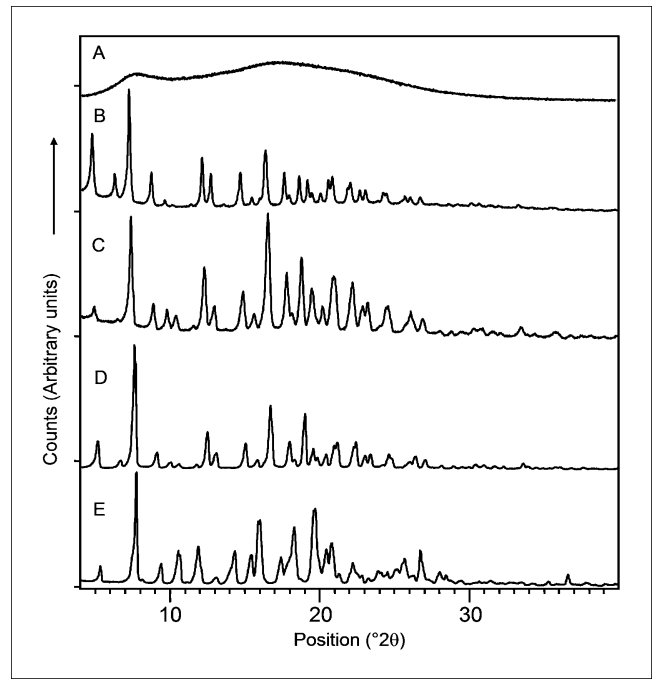

Fig. 2: PXRD diffractograms of commercial lopinavir (A), needles from diethyl ether (B), resin from chloroform (C) and crystals from ethyl acetate (D) and acetone (E)

Unfortunately, the exact crystalline content, usually determined using the methods described by Lefort et al. (2004) and Black and Lovering (1977), could not be reliably performed in this in this study, because of the absence of a 100% crystalline sample. However, birefringence could still be used to visualize the crystallites present in the more amorphous samples, e.g. the resin

Table 1: Values of T_β and T_g when heated at 10 K/min (mean ± S.D.), activation energies for β- and α-processes and the fragility (m) and strength (D) parameters of each sample

Preparation conditions	T_β (K) 10 K/min	T_g (K) 10 K/min	ΔE (kJ/mol) T_β	T_β^{mid}	T_g	T_g^{mid}	m	D
Lopinavir	330 ± 1.56	348 ± 0.41	557	325	144	140	21	106
Ethyl acetate	331 ± 0.23	346 ± 0.67	–	–	–	–	–	–
Acetone	331 ± 1.24	350 ± 0.06	–	–	–	–	–	–
Diethyl ether	329 ± 0.17	340 ± 2.36	372	251	217	126	33	34
Chloroform	329 ± 1.64	339 ± 2.82	250	211	203	165	31	39
Dichloromethane	329 ± 1.72	331 ± 6.61	368	294	133	94	20	130
AG	301 ± 1.04	318 ± 0.08	45	26	302	340	50	17
QG	318 ± 0.66	351 ± 0.39	334	273	453	275	67	11

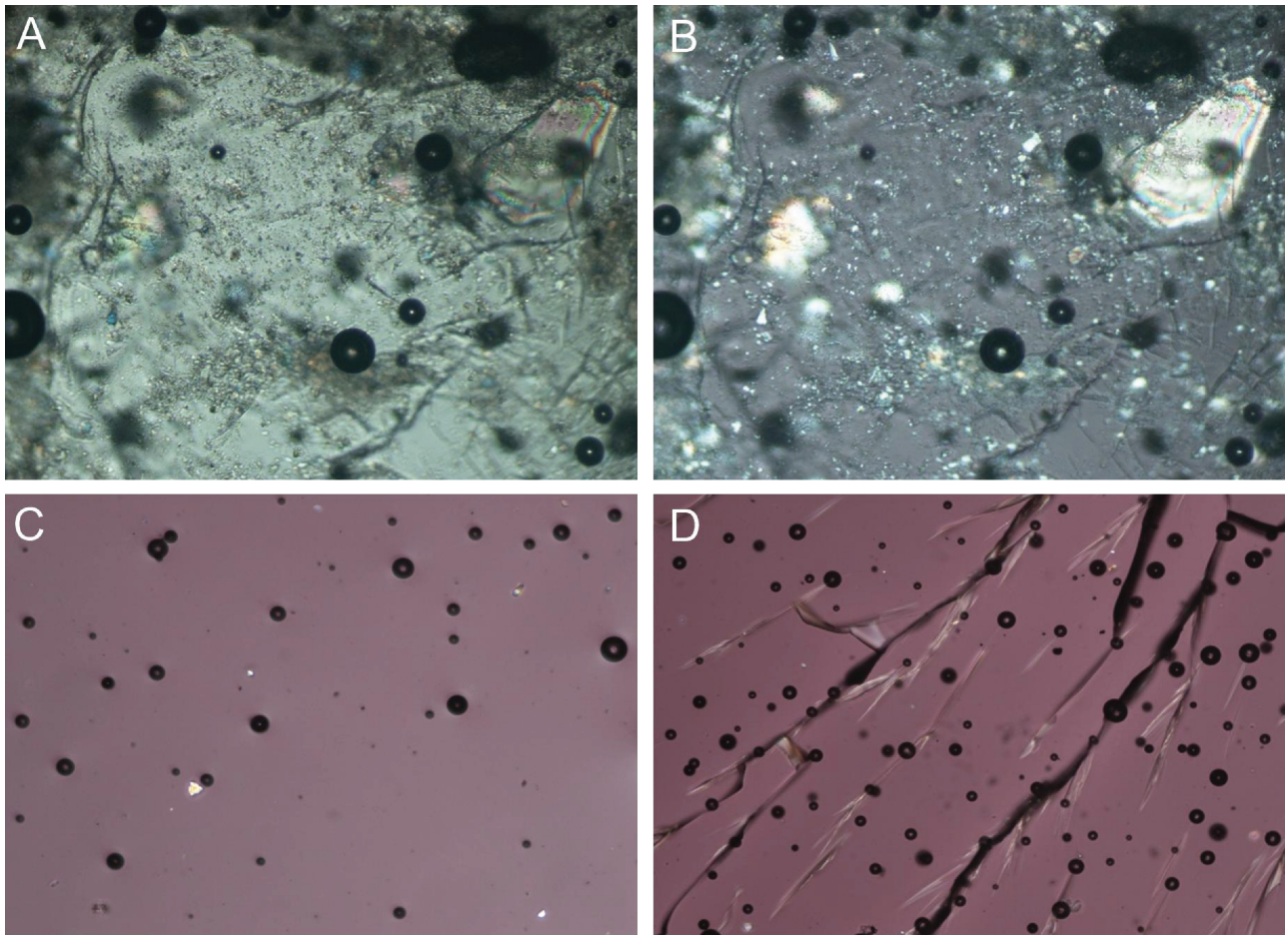

Fig. 3: Micrograms of lopinavir resin from chloroform (A and B), AG (C) and QG (D), where birefringence was used in B, C and D to visualize the crystallites embedded in the amorphous matrixes

from chloroform and the glasses obtained from cooling of the melt (Fig. 3).

Results from the β-relaxation and fragility studies are presented in Table 1. The extremely fragile behavior observed for the lopinavir crystals from acetone and ethyl acetate ($m = 561$ and 880 respectively) can be attributed to their small amounts of amorphous content (Figs. 1 and 2). Due to their small size, these amorphous regions undergo rapid changes at T_β and T_g, causing almost undetectable shifts in T_β and T_g with regards to the heating rate. This in turn, increases the slopes of their Arrhenius plots, and therefore their respective activation energies, resulting in unusually high values of ΔE. This could probably be remedied by increasing the sample size. However, such an increase would require larger samples than what could be contained in a DSC crucible. This represents a shortcoming in the method, which was originally developed for glasses prepared from cooling of the melt, yielding highly amorphous samples (Vyazovkin and Dranca 2006; Crowley and Zografi 2001). It appears that once the crystalline content exceeds a certain point, these methods are no longer valid for determining ΔE_β and ΔE_{Tg}. For these reasons, the data is excluded from Table 1 and Fig. 4 and no conclusions will be drawn from these ΔE values.

The differences in crystalline content, as seen from the PXRD data (Fig. 2), between the lopinavir resins prepared in this study can also be elucidated by their differences in ΔE_β (Table 2). The gum-like properties of a resin, coupled with its long setting time, offer significantly more freedom for molecular motion than a glass or crystal. In resins, local regions with energies exceeding that of ΔE_β can offer sufficient molecular mobility for nucleation to occur, leading to the random distribution of crystallites observed in the resin from chloroform (Fig. 3). Commercial lopinavir displayed the highest ΔE_β of all the amorphous samples, explaining its stability and resistance to crystallization following shipping, handling and storage for extended periods of time at temperatures below T_g.

Table 2: Aqueous solubility (mean ± S.D.) of commercial lopinavir, its glasses and recrystallization products

Preparation conditions	Solubility (μg/mL)
Commercial lopinavir	54.3 ± 0.7
Ethyl acetate	20.4 ± 0.7
Acetone	24.7 ± 0.6
Diethyl ether	55.3 ± 0.4
Chloroform	57.9 ± 0.9
Dichloromethane	25.6 ± 0.2
AG	93.7 ± 0.9
QG	35.2 ± 0.6

AG exhibited the highest aqueous solubility (Table 2), followed by the resin obtained from chloroform, while other predominantly amorphous samples, e.g. QG and the resin obtained from dichloromethane, displayed solubility values only slightly higher than those of the crystalline samples. As expected, the predominantly amorphous lopinavir samples displayed enhanced aqueous solubility when compared to their more crystalline counterparts.

Based on their physical properties, the crystals from ethyl acetate, QG and AG were chosen for dissolution studies. These samples shared the ability to be broken (without being totally crushed), and sieved to obtain a similar particle size distribu-

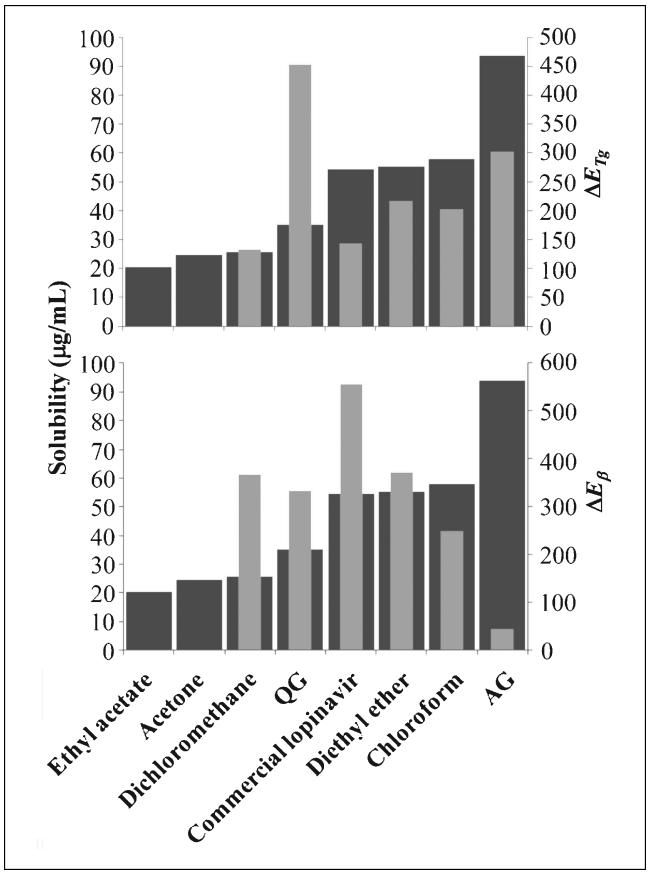

Fig. 4: Correlation between solubility (primary y-axis, dark grey) and ΔE_{Tg} and ΔE_{β} (secondary y-axis, light grey) respectively

tion, thereby eliminating an important variable that could affect dissolution rate. The gum-like properties of the resins made it impossible for them to be broken down into smaller pieces with a similar size distribution to that of the above mentioned samples. By maintaining the chemical structure, particle size distribution, analysis temperature, stirring rate and dissolution medium, differences in dissolution rate can more readily be attributed to the stability of the system. The dissolved concentrations were expressed as cumulative dissolved fractions (α) and straight line regions of the curves (Fig. 5), consisting of α values ranging from 0.1 to 0.8, were fitted against deceleratory kinetics models presented in Table 3. These linear regions represent dissolution under sink conditions. Results from the model fitting

Table 3: Rate equations of deceleratory kinetic models (Brown et al. 1980)

Model	Integral form $g(\alpha) = kt$
Sigmoid rate equations	
Avarami-Erofe'ev (A2)	$[-\ln(1 - \alpha)]^{1/2}$
Avarami-Erofe'ev (A3)	$[-\ln(1 - \alpha)]^{1/3}$
Avarami-Erofe'ev (A4)	$[-\ln(1 - \alpha)]^{1/4}$
Diffusion models	
One-dimensional diffusion (D1)	α^2
Two-dimensional diffusion (D2)	$[(1 - \alpha)\ln(1 - \alpha)] + \alpha$
Three-dimensional diffusion (D3)	$[1 - (1 - \alpha)^{1/3}]^2$
Ginstling-Brounshtein (D4)	$1 - (2\alpha/3) - (1 - \alpha)^{2/3}$
Reaction-order models	
First-order (F1)	$-\ln(1 - \alpha)$
Second-order (F2)	$(1 - \alpha)^{-1} - 1$
Third-order (F3)	$0.5((1 - \alpha)^{-2} - 1)$

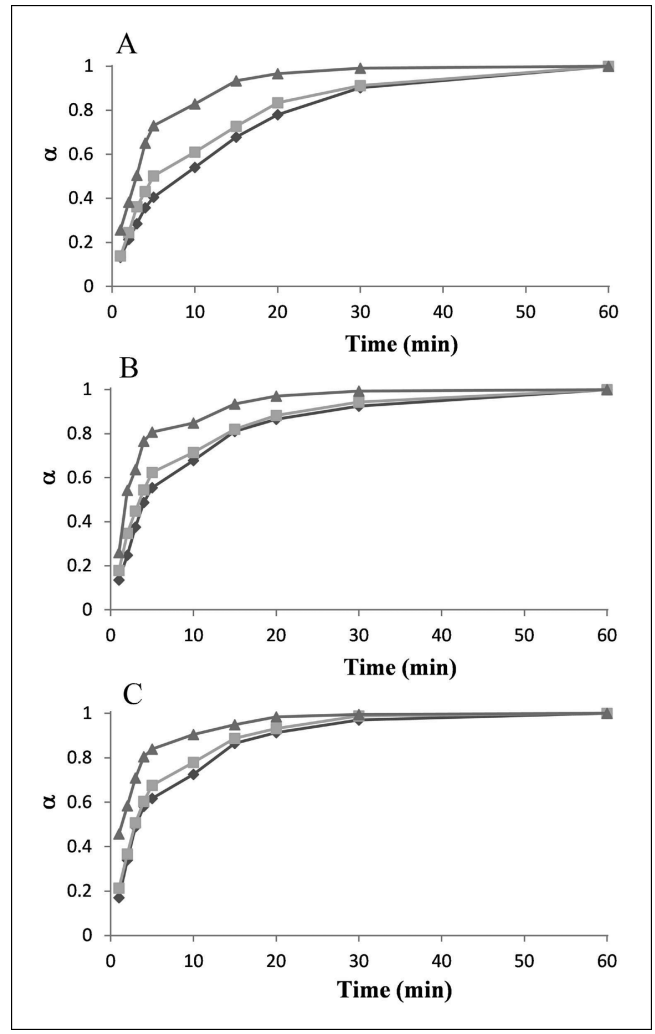

Fig. 5: Dissolution curves of lopinavir crystals from ethyl acetate (A), QG (B) and AG (C) at 298 K (diamonds), 308 K (squares) and 318 K (triangles)

indicated that the dissolution process followed first-order kinetics ($R^2 = 0.998$). From the dissolution rate constants, the ΔE_{Diss} for the lopinavir crystals, QG and AG were determined as 36, 22 and 18 kJ/mol respectively.

3. Discussion

As expected, the inherent structural flexibility of lopinavir and its capacity to undergo extensive hydrogen bonding led to a solid-state system presenting multiple metastable forms with varying degrees of disorder, evident from the differences in T_g. A physicochemical analysis of lopinavir, its glasses and recrystallization products was undertaken to obtain several parameters which are known to be indicative of differences in the stability of a system, e.g. ΔE_{Tg}. During the course of the analyses, several incidents where stability would have been wrongfully assigned if only considering ΔE_{Tg} became clear, e.g. commercial lopinavir would have been dubbed the second most unstable lopinavir sample (ΔE_{Tg} 144 kJ/mol). However, it is stable for extended periods of time and is resistant to crystallization following handling, while the resin obtained from chloroform displayed a higher ΔE_{Tg} value of 203 kJ/mol and formed large amounts of crystallites in its amorphous matrix, even while stored well below T_g. In both these cases the true physical stability could be deduced from ΔE_{β} (Table 1). Despite having a similar macroscopic appearance, the resins from chloroform and dichloromethane displayed vastly different physicochemi-

cal profiles, especially concerning crystalline content. The resin obtained from chloroform had a large amount of crystalline content (Figs. 2 and 3) after one month of storage, while the resin obtained from dichloromethane still displayed only a diffuse halo on its PXRD (not shown). These differences in crystalline content while stored at temperatures below T_g can be attributed to ΔE_β, where the lower molecular mobility energy barrier imposed on the resin obtained from chloroform possibly facilitated the formation of crystallites in its amorphous matrix.

Thermal analyses indicated that each solid-state system displayed its own unique T_g and fragility parameters, suggesting that each system is a unique metastable form of lopinavir. This observation was supported by the fact that each sample was analyzed one month after preparation and all samples were stored under similar conditions. Another method of assessing the stability of a system is solubility studies, where unstable systems display higher equilibrium solubility values than their more stable counterparts. By maintaining the chemical structure, physicochemical properties, like solubility, can be readily attributed to the stability of the system. Relating the solubility data to the physicochemical parameters obtained from thermal analyses gave the well known trend in which the solubility increases when moving from crystalline to amorphous systems. However, amongst the amorphous samples the solubility did not increase with increasing amorphous content, as deduced from PXRD (Fig. 4). The best correlation was found between solubility and ΔE_β. Interestingly, the ΔE_{Diss} values of the lopinavir samples analyzed exhibited the same trend as their respective ΔE_β values, suggesting that the lower activation energy barrier imposed by lower values of ΔE_β might facilitate the removal of molecules from the solid's surface, thereby decreasing the amount of energy needed to dissolve the sample and increasing its dissolution rate. However, more future studies will have to be carried out before drawing any conclusions from this potential correlation between ΔE_β and ΔE_{Diss}. The solubility and dissolution data support the conclusions drawn from the thermal analyses; that each preparation is a unique metastable form of commercial lopinavir.

In this work, we reported several novel solid-state forms of the peptidomimetic drug lopinavir, and illustrated the ability of a chemical species to rearrange into several metastable solid-state forms, independently existing under similar conditions for up to one month (and possibly even longer). This observation emphasizes the need for pharmaceutical scientists to perform a thorough physical chemical analysis on a drug in order to obtain a true representation of its solid-state properties. Combining several analytical techniques and methods to evaluate the systems, made it clear that each of these metastable forms prepared in this study displayed its own unique physicochemical behavior and stability. The knowledge obtained from this study, e.g. the enhanced aqueous solubility of the lopinavir glass obtained from cooling of the melt under ambient conditions, can assist in future research and formulation of lopinavir and similar peptidomimetic drugs.

4. Experimental

4.1. Materials

Lopinavir (HPLC assay > 99%) was purchased from Dr, Reddy's Laboratories Ltd., Andhra Pradesh, India.

4.2. Methods

4.2.1. Differential scanning calorimetry (DSC)

DSC experiments were carried out on a Shimadzu DSC-60A (Shimadzu, Japan). The DSC cell was purged with nitrogen at a flow rate of 35 mL/min. Indium and tin standards were used to calibrate the temperature and heat of fusion. All samples were accurately weighed (5–6 mg) and analyzed in aluminum pans with pierced lids to facilitate potential volatile evolution during heating. The data was analyzed using ta60 software version 2.11.

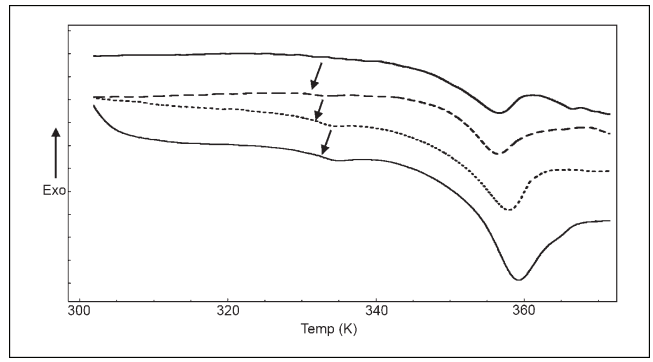

Fig. 6: DSC overlay of commercial lopinavir before annealing (thick solid), and after annealing showing the shifts in β-relaxations at heating rates of 10 K/min (dashed), 15 K/min (dotted) and 20 K/min (thin solid)

To investigate β-relaxations, the optimum conditions were found to be an annealing time of 20 min at a temperature of 0.8 T_g, consistent with known literature (Vyazovkin and Dranca 2006). Because of the inherently small endothermic peaks associated with β-relaxations, heating rates of 10, 15 and 20 K/min were used. These heating rates were experimentally chosen based on observations that rates < 10 K/min resulted in extensive oscillation between enthalpy loss and recovery, making accurate data collection troublesome, making 10 K/min the slowest heating rate. Rates > 20 K/min led to overlap of the β- and α-processes, again resulting in unreliable β-relaxation values and making 20 K/min the highest heating rate used in this study. T_β was taken as the onset temperature of the relaxation, measured using the same extrapolation technique used in T_g determination (Crowley and Zografi 2001). Figure 6 illustrates the small endothermic peaks (relative to the α-processes) of the β-relaxations obtained after annealing, as well as the shifts in onset temperatures with regard to different heating rates. The positions of these peaks, along with their thermal behavior, are consistent with other DSC-based β-relaxation investigations (Vyazovkin and Dranca 2006). To investigate α-relaxations, the samples were annealed for 10 min at temperatures 20 K above T_g (Crowley and Zografi 2001). The samples were analyzed at heating rates of 5, 10 and 20 K. For both the β- and α-relaxations similar cooling and reheating rates were maintained (Crichton and Moynihan 1988; Moynihan et al. 1974).

The activation energies for local and global molecular mobility were calculated from non-isothermal DSC data using eq. 1 (Vyazovkin and Dranca 2006; Crowley and Zografi 2001).

$$\frac{-\Delta E_a}{R} = \frac{d(\ln q)}{d({T_g}^{-1})} \tag{1}$$

Where the activation energy (ΔE_a) can be written as ΔE_β, for local relaxations, and ΔE_{Tg} for global relaxations. From ΔE_{Tg} the m values were calculated according to eq. 2 (Crowley and Zografi 2001).

$$m = \frac{\Delta E_{Tg}}{(\ln 10) R T_g} \tag{2}$$

The minimum value of m (m_{min}) was determined to be 16, and from that the D value of each sample was calculated using eq. 3 (Crowley and Zografi 2001).

$$D = \frac{(\ln 10) {m_{\min}}^2}{(m - m_{\min})} \tag{3}$$

4.2.2. Thermogravimetric analysis (TGA)

TGA experiments were performed using a Shimadzu DTG-60 (Shimadzu, Japan). The TGA chamber was purged with nitrogen at 35 mL/min. Indium and tin standards were used to calibrate the temperature. All samples were accurately weighed (7–8 mg) and analyzed in open aluminum pans. The data was analyzed using ta60 software version 2.11.

4.2.3. Fourier transform infrared spectroscopy (FTIR)

FTIR analyses were performed using a Shimadzu IRPrestige-21 (Shimadzu, Japan). Peak positions were confirmed using polystyrene film. Spectra were recorded over a range of 500−4000 cm^{-1}. All samples were accurately weighed (4–5 mg) and homogeneously dispersed in a ground matrix of KBr. The data was analyzed using Shimadzu IRsolution software version 1.40.

4.2.4. Ultraviolet-visible absorption spectrophotometry (UV-Vis)

UV-vis analyses were carried out on a Shimadzu UV-1800 (Shimadzu, Japan). Analyses were conducted at 210 nm in quartz cuvettes using Shimadzu UVProbe software version 2.32.

4.2.5. Hot stage microscopy

Hot stage micrographs were taken on a Nikon Eclipse E400 microscope (Nikon, Japan) equipped with a Nikon DS-Fi1 camera and cross-polarized light filter. Images were acquired with NIS-Elements software version 3.22.

4.2.6. Powder X-ray diffraction (PXRD)

PXRD analyses were carried out on a PANalytical X'Pert Pro (PANalytical, Netherlands). Measurement conditions were: Anode, Cu; $K\alpha_1$, 1.5405 Å; $K\alpha_2$, 1.54443 Å; K-Beta, 1.39225 Å; $K\alpha_1/K\alpha_2$ ratio, 0.5; Generator settings, 40 mA, 45 kV; divergence slit, 0.957°, fixed; step size, 0.017 ° in 2θ; scan step times, 19.685 s; temperature, 25 °C. The data was analyzed using X'Pert Data Collector software version 4.0A.

4.2.7. Solubility

Aqueous solubility of each sample was determined by stirring a supersaturated solution of each prepared material at 310 K for 24 h to reach equilibrium solubility. Concentrations were determined by measuring the UV-vis absorbance. Linearity was observed in the range 0.01 to 200 μg/mL.

4.2.8. Dissolution

To control the particle size distribution, samples were sieved and the fraction between 400 – 1400 μm collected. Accurately weighed (54 – 56 mg) amounts of these samples were dissolved in 10 mL double distilled water at 298, 308 and 318 K over 4 h. Initial withdrawals were made at 1 minute intervals for the first 5 min, followed by longer time intervals and analyses were carried out using UV-vis absorbance.
Normalized cumulative dissolved fractions (α) were fitted against deceleratory kinetics models (Table 3) and the rate constants (k) thereby obtained were used to determine the activation energy of dissolution (ΔE_{Diss}) for each sample using the well-known Arrhenius equation (Eq. 4).

$$k = Ae^{-\left(\frac{\Delta E_{Diss}}{RT}\right)} \quad (4)$$

Where A is the frequency factor and R the gas constant.

Acknowledgements: The authors thank the North-West University and the National Research Foundation (NRF) of South Africa for funding this work.

References

Aasland S, McMillan PF (1994) Density-driven liquid–liquid phase separation in the system AI_2O_3-Y_2O_3. Nature 369: 633–636.

Alie J, Menegotto J, Cardon P, Duplaa H, Caron A, Lacabanne C, Bauer M (2004) Dielectric study of the molecular mobility and the isothermal crystallization kinetics of an amorphous pharmaceutical drug substance. J Pharm Sci 93: 218–233.

Alig I, Braun D, Langendorf R, Voigt M, Wendorff JH (1997) Simultaneous ageing and crystallization processes within the glassy state of a low molecular weight substance. J Non-Cryst Solids 221: 261–264.

Bhugra C, Shmeis RA, Krill SL, Pikal MJ (2008) Prediction of onset of crystallization from experimental relaxation times. II. Comparison between predicted and experimental onset times. J Pharm Sci 97: 455–472.

Black DB, Lovering EG (1977) Estimation of the degree of crystallinity in digoxin by X-ray and infrared methods. J Pharm Pharmacol 29: 684–687.

Brown WE, Dollimore D, Galwey AK (1980) Theory of solid state reaction kinetics. In: Bamford CH, Tipper CFH (eds.) Comprehensive Chemical Kinetics, vol. 22, Amsterdam, pp. 41–113.

Crichton SN, Moynihan CT (1988) Dependence of the glass transition temperature on heating rate. J Non-Cryst Solids 99: 413–417.

Crowley KJ, Zografi G (2001) The use of thermal methods for predicting glass-former fragility. Thermochim Acta 380: 79–93.

Dantuluri AKR, Amin A, Bansal AK (2011) Role of α-relaxation on crystallization of amorphous celecoxib above T_g probed by dielectric spectroscopy. Mol Pharm 8: 814–822.

Ediger MD (2000) Spatially heterogeneous dynamics in supercooled liquids. Annu Rev Phys Chem 51: 99–128.

Elamin AA, Alderborn G, Ahlneck C (1994) The effect of pre-compaction processing and storage conditions on powder and compaction properties of some crystalline materials. Int J Pharm 108: 213–224.

Graeser KA, Patterson JE, Zeitler JA, Gordon KC, Rades T (2009) Correlating thermodynamic and kinetic parameters with amorphous stability. Eur J Pharm Sci 37: 492–498.

Grzybowska K, Paluch M, Grzybowski A, Wojnarowska Z, Hawelek L, Kolodziejczyk K (2010) Molecular dynamics and physical stability of amorphous anti-inflammatory drug: celecoxib. J Phys Chem B 114: 12792–12801.

Hancock BC, Dalton CR, Pikal MJ, Shamblin SL (1998) A pragmatic test of a simple calorimetric method for determining the fragility of some pharmaceutical materials. Pharm Res 15: 762–767.

Hancock BC, Parks M (2000) What is the true solubility advantage of amorphous pharmaceuticals? Pharm Res 17: 397–404.

Hikima T, Hanaya M, Oguni M (1999) Microscopic observation of a peculiar crystallization in the glass transition region and β-process as potentially controlling the growth rate in triphenylethylene. J Mol Struct 479: 245–250.

Hüttenrauch R (1978) Molecular pharmaceutics as a basis of modern pharmaceutical technology. Acta Pharm Technol Suppl 6: 55–127.

Kempf DJ, Marsh KC, Kumar G, Rodrigues AD, Denissen JF, McDonald E, Kukulka MJ, Hsu A, Granneman GR, Baroldi PA, Sun E, Pizzuti D, Plattner JJ, Norbeck DW, Leonard JM (1997) Pharmacokinetic enhancement of inhibitors of human immunodeficiency virus protease by coadministration with ritonavir. Antimicrob Agents Chemother 41: 654–660.

Lefort R, De Gusseme A, Willart F-J, Danède F, Descamps M (2004) Solid state NMR and DSC methods for quantifying the amorphous content in solid dosage forms: an application to ball-milling of trehalose. Int J Pharm 280: 209–219.

Levine H, Slade L (1988) Thermomechanical properties of small-carbohydrate–water glasses and 'rubbers'. Kinetically metastable systems at sub-zero temperatures. J Chem Soc Faraday Trans 84: 2619–2633.

Lordi N, Shiromani P (1984) Mechanism of hardness of aged compacts. Drug Dev Ind Pharm 10: 729–752.

Mahlin D, Ponnambalam S, Höckerfelt MH, Bergström CAS (2011) Toward *in silico* prediction of glass-forming ability from molecular structure alone: a screening tool in early drug development. Mol Pharm 8: 498–506.

Mitchell AG, Down GRB (1984) Recrystallization after powder compaction. Int J Pharm 22: 337–344.

Moynihan CT, Easteal AJ, Wilder J, Tucker J (1974) Dependence of the glass transition temperature on heating and cooling rate. J Phys Chem 78: 2673–2677.

Ngai KL (2003) An extended coupling model description of the evolution of dynamics with time in supercooled liquids and ionic conductors. J Phys: Condens Matter 15: S1107–S1125.

Qi S, Avalle P, Saklatvala R, Craig DQM (2008) An investigation into the effects of thermal history on the crystallization behavior of amorphous paracetamol. Eur J Pharm Biopharm 69: 364–371.

Safrin S (2004) Antiviral agents. In: Katzung BG (ed.) Basic and clinical pharmacology, 9th ed., Singapore, pp. 801–827.

Stillinger FH (1995) A topographic view of supercooled liquids and glass formation. Science 267: 1935–1939.

Surana R, Pyne A, Suryanarayanan R (2004) Effect of preparation method on physical properties of amorphous trehalose. Pharm Res 21: 1167–1176.

Vyazovkin S, Dranca I (2005) Physical stability and relaxation of amorphous indomethacin. J Phys Chem B 109: 18637–18644.

Vyazovkin S, Dranca I (2006) Probing beta relaxation in pharmaceutically relevant glasses by using DSC. Pharm Res 23: 422–428.

Vyazovkin S, Dranca I (2007) Effect of physical aging on nucleation of amorphous indomethacin. J Phys Chem B 111: 7283–7287.

Ward GH, Schultz RK (1995) Process-induced crystallinity changes in albuterol sulfate and its effect on powder physical stability. Pharm Res 12: 773–779.

Weuts I, Kempen D, Six K, Peeters J, Verreck G, Brewster M, Van Den Mooter G (2003) Evaluation of different calorimetric methods to determine glass transition temperature and molecular mobility below T_g for amorphous drugs. Int J Pharm 259: 17–25.

Yoshioka S, Miyazaki T, Aso Y (2006) β-relaxation of insulin molecule in lyophilized formulations containing trehalose or dextran as a determinant of chemical reactivity. Pharm Res 23: 961–966.

Yoshioka S, Miyazaki T, Aso Y, Kawanishi T (2007) Significance of local mobility in aggregation of β-galactosidase lyophilized with trehalose, sucrose or stachyose. Pharm Res 24: 1660–1667.